OPTICAL NANOBIOSENSING OF STIBOGLUCONATE IN PLASMA AND URINE USING GREEN SYNTHESIZED FLUORESCENT CARBON NANODOTS**

W. Talaat, A. F. Hassan*

Damanhour University, Damanhour 25111, Egypt;
e-mail: asmz68@sci.dmu.edu.eg, asmz68@yahoo.com

Fluorescent carbon nanodots were synthetized from garlic peels as optical nanobiosensors for an anti-leishmaniotic stibogluconate drug. The characterization techniques for the synthetized carbon nanodots confirmed its thermal stability, nanosize in the range 2—14 nm, amorphous nature, and the presence of C–O functional groups. The optical sensor, based on the fluorescent nature of carbon nanodots, was developed for the drug nanobiosensor in dosage form and in human biological fluids. The drug was digested to release a pentavalent antimony cation that quenches the fluorescence intensity of carbon nanodots. The extraction method was performed through ion pairing with trinonylamine. The optical sensing was extended to the in vivo analysis of stibogluconate in real human plasma. The sensing of stibogluconate was found to be linear over the range 0.01–0.10 μg/mL with percentage recoveries of 99.25±1.86, and 99.624±1.33 in vials with spiked plasma and in spiked urine.

Keywords: *garlic peels, carbon nanodots, optical sensor, biosensing, dosage form, real plasma.*

ОПТИЧЕСКОЕ НАНОБИОСЕНСИРОВАНИЕ СТИБОГЛЮКОНАТА В ПЛАЗМЕ КРОВИ И УРИНЕ ЧЕЛОВЕКА С ИСПОЛЬЗОВАНИЕМ ФЛУОРЕСЦЕНТНЫХ УГЛЕРОДНЫХ НАНОТОЧЕК, СИНТЕЗИРОВАННЫХ ЭКОЛОГИЧНЫМ “ЗЕЛЕНЫМ” МЕТОДОМ

W. Talaat, A. F. Hassan*

УДК 535.37;620.3

Университет Даман-Хур, Даманхур, 25111, Египет;
e-mail: asmz68@sci.dmu.edu.eg, asmz68@yahoo.com

(Поступила 14 октября 2019)

Из кожуры чеснока синтезированы флуоресцентные углеродные наноточки в качестве оптического нанобиозонда для антилейшманиотического препарата стибоглюконата. Методы характеризации синтезированных углеродных наноточек подтвердили их термостойкость, наноразмерность в диапазоне 2–14 нм, аморфную природу и присутствие функциональных групп С–О. Разработан основанный на флуоресцентной природе углеродных наноточек оптический сенсор для нанобиозондирования лекарственных препаратов в таблетированной форме и биологических жидкостях человека. Препарат переваривали с высвобождением пятивалентного катиона сурьмы, который тушит флуоресценцию углеродных наноточек. Экстракция осуществлялась путем образования ионной пары с триноніламином. Анализ стибоглюконата оптическим методом осуществлен in vivo в реальной плазме человека. Характеристика обнаружения стибоглюконата линейная в пределах 0.01–0.10 мкг/мл при воспроизводимости 99.25±1.86 и 99.624±1.33 с добавленными плазмой крови и уриной.

Ключевые слова: *чесночные пилинги, углеродные наноточки, оптический датчик, биосенсор, лекарственная форма, реальная плазма.*

** Full text is published in JAS V. 88, No. 2 (http://springer.com/journal/10812) and in electronic version of ZhPS V. 88, No. 2 (http://www.elibrary.ru/title_about.asp?id=7318; sales@elibrary.ru).

Introduction. Recently, carbon nanodots, exhibiting the attractive properties of low cost, good water solubility, biocompatibility, high stability, low toxicity, and high photoluminescence, have been synthesized. The presence of many carboxylic groups on the surface of carbon nanodots is responsible for its water solubility and biocompatibility [1–3]. The mechanism of fluorescence is under debate, and some articles suggest that the electronic transition through quantum confinement is responsible for the emission [4, 5]. Others believe that the surface defects or the surface trapped charges are the reason for the fluorescence [6, 7]. The fluorescence of carbon nanodots makes it suitable for optical sensing. It has been reported that the fluorescence of carbon nanodots is quenched by heavy metals and some organic compounds, for example, amines. This effect opens the door towards new optical sensors of heavy metals such as mercury and copper [8, 9] in addition to the sensing of amino compounds like nucleic acid and organic compounds like pollutants [10, 11]. Moreover, it was observed that the fluorescence of carbon nanodots is highly sensitive to pH [12].

Stibogluconate has the formula 2,4:2',4'-O-(oxydistibylidyne) bis (D-gluconic acid) [13] and is used to treat leishmaniasis.

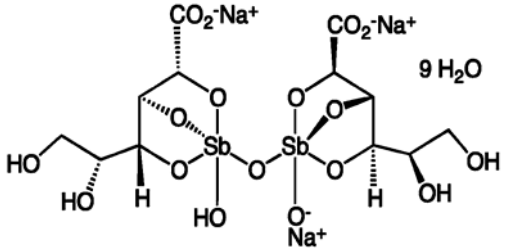

The mechanism of sodium stibogluconate is poorly understood but is thought to stem from the inhibition of macromolecular synthesis via a reduction in available ATP and GTP, likely secondary to inhibition of the citric acid cycle and glycolysis. To the best of our knowledge, few methods have been reported for the analysis of stibogluconate in the literature. The first method was reported in the British Pharmacopoeia [14]. Another method was reported for the determination of pentavalent antimony in sodium stibogluconate via a redox reaction with acidified iodide to liberate iodine, which is monitored spectrophotometrically at 350 nm [15]. The determination of inorganic and organic antimony(V) was studied by many researchers using different techniques. A soil sample containing organic and inorganic antimony was determined using HG-AFS (hydride generation atomic fluorescence spectrometry) with a detection limit of 0.9 ng/g and a quantification value of 3.1 ng/g [16]. The electrothermal atomic absorption method was used to determine antimony(III, V) soluble in an aqueous medium after using carbon nanotubes for solid-phase extraction procedures, where the detection limit was found to be 0.05 μg/L [17]. A liquid–liquid extraction flow analysis automated system was used to determine the concentration of Sb(V) in antileishmanial drugs studied on the basis of the formation of an ion pair between a rhodamine B cation and a hexachloroantimonate anion in toluene [18]. Hydride generation-four-channel nondispersive atomic fluorescence spectrometry, electrothermal atomic absorption spectrometry, and the kinetic data of voltammetric measurements methods were developed to determine the concentration of antimony in biological samples with observable detection limits of 0.04, 3.9, and 20.0 ng/mL, respectively [19–21].

We introduce a novel method for the determination of stibogluconate either in dosage form or in human biological fluids. The method is based mainly on the preparation of fluorescent carbon nanodots from a green source of carbon atoms (garlic peels) and the quenching effect of antimony.

Materials and methods. Sodium stibogluconate was purchased from Sigma Aldrich, Germany, and its purity was estimated using the comparison method [14] and found to be 99.85±0.32. Trinonylamine (98%) was purchased from ChemSpider, London, UK, and its solution (10%) was prepared in *n*-hexane. Sulfuric acid, hydrochloric acid, ammonia, and *n*-hexane were purchased from El-Nasr Pharmaceutical Chemicals Co., Egypt and used without further treatment. Pentostam® vials, each labeled to contain 100 mg/mL of pentavalent antimony, Batch No. 102-10-24710, were produced by GlaxoSmithKline and obtained from a local pharmacy. All the solvents used were of HPLC grade.

Carbon nanodots were synthetized by the method described by Gaber et al. [22] with slight modifications. Garlic peels were cleaned with deionized water and dried for 3 h at 60°C. The dried material was ground into pieces of about 0.5 mm. Ten grams of the ground dried materials was added into a cleaned dried crucible and heated for 2 h at 250°C in atmospheric oxygen. The residue was then dissolved in 20 mL of Milli-Q water and filtered through a 0.45 μm nylon filter. The filtrate was purified via a dialyzer tube for 2 days using MWCO, 3.5 KDa.

Carbon nanodots were investigated using different techniques. A Shimadzu DTA-50 (Japan) was used for the investigation of the thermogravimetric analysis curve (TGA) of carbon nanodots from room temperature to 900°C. The X-ray diffraction pattern (XRD) was investigated using PANalytical X'Pert PRO, CuK_α radiation (λ = 1.5405 Å) in the 2θ range of 5–80° where the tube was operated at 30 kV. Transmission electron microscopy (TEM) and energy dispersive X-ray spectra (EDX) were studied at an acceleration voltage of 200 kV using a JEOL-JEM-2100 (Tokyo, Japan). Fourier transform infrared spectroscopy (FTIR) was applied using a Mattson 5000 FTIR spectrometer in the range 400–4000 cm^{-1}.

A Cary Eclipse fluorescence spectrophotometer (Agilent Technologies, Germany) with a 1 cm quartz cell was used for all measurements. The slit width of both the excitation and emission monochromators was set at 1.5 nm. The systematic errors in the measurement of the stibogluconate concentration by the Cary Eclipse fluorescence spectrophotometer were ±0.10%. Every measurement was repeated three times to obtain the average values. The calibration and linearity of the instrument were often checked with standard quinine sulfate (0.01 μg/mL) at λ_{ex} = 302 nm and λ_{em} = 420 nm as the excitation and emission wavelengths.

Ten milligrams of carbon nanodots was dissolved in a mixture of deionized water/methanol (50:50) and diluted with the same mixture to 25 mL in a 25 mL clean and dry volumetric flask. Ten milligrams of sodium stibogluconate was dissolved in deionized water and diluted to 100 mL in a 100 mL volumetric flask to get the standard solution. The solution stability was confirmed for at least one week with keeping in the refrigerator. Re-analyzing the data of the sample proves that there is no indication of any change of carbon nanodots.

General analytical procedures. Construction of the calibration curve. A half milliliter of the carbon nanodots standard solution was transferred to a 10-mL volumetric flask to obtain a final concentration of 20 μg/mL. The solution was diluted to the mark with a mixture of deionized water and methanol (50:50). The emission fluorescence intensity of the previous solution was measured at 420 nm after excitation at 302 nm.

Aliquots of the sodium stibogluconate standard solution were refluxed with 8 mL of concentrated sulfuric acid for 45 min in a 10 mL volumetric flask, cooled to room temperature, and completed to the mark with deionized water. One milliliter of the previous solution was mixed with a half milliliter of the carbon nanodots standard solution and 5 mL of the diluting mixture in a 10 mL beaker. The pH of the solution was adjusted to 3.0 with ammonia, and the solution was quantitatively transferred to a 10 mL volumetric flask and diluted to 10 mL with the diluting mixture to achieve the required concentration range (0.01–0.10 μg/mL). The emission fluorescence intensity of the previous solutions was measured at 420 nm after excitation at 302 nm. A calibration curve was constructed by plotting the concentration of sodium stibogluconate versus the emission intensity with the development of the regression equation.

Optical sensing of sodium stibogluconate in the vial. One milliliter of the vial content (equivalent to 100 mg of antimony) was diluted to 100 mL in a 100 mL volumetric flask. Aliquots of the diluted solution were refluxed with 8 mL of concentrated sulfuric acid for 45 min in a 10 mL volumetric flask, cooled to the room temperature, and completed to the mark with deionized water. One milliliter of the previous solution was mixed with a half milliliter of the carbon nanodots standard solution and 5 mL of the diluting mixture in a 10 mL beaker. The pH of the solution was adjusted to 3.0 with ammonia, and the solution was quantitatively transferred to a 10 mL volumetric flask and diluted to 10 mL with the diluting mixture to achieve the required concentration range (0.01–0.10 μg/mL). The emission fluorescence intensity of the previous solution was measured at 420 nm after excitation at 302 nm. The nominal concentration was obtained from the calibration curve or the corresponding regression equation.

Optical biosensing of sodium stibogluconate. Control test of unspiked plasma and urine. The control test of unspiked plasma and urine was essential to prove that the plane plasma and urine exhibit no interference at the tested emission wavelength (420 nm). One milliliter of the blank matrix of the plasma or urine sample was added into a series of centrifuge tubes and treated with 1 mL of 0.01 M HCl and 1 mL of 10% solution trinonylamine in *n*-hexane. The samples were centrifuged at room temperature for 30 min at 4000 rpm. The hexane layer was separated and evaporated till dry under nitrogen gas. The residue was digested with 8 mL of concentrated sulfuric acid for 45 min in 10 mL volumetric flasks, cooled to room temperature, and completed to the mark with deionized water. One milliliter of the previous solution was mixed with a half milliliter of the carbon nanodots standard solution and 5 mL of the diluting mixture in a 10 mL beaker. The pH of the solution was adjusted to 3.0 with ammonia, and the solution was quantitatively transferred to a 10 mL volumetric flask and diluted to 10 mL with the diluting mixture. The emission fluorescence intensities of the previous solutions were measured at 420 nm after excitation at 302 nm. The control experiment indicated that no significant quenching in the carbon nanodots emission intensity, proving that there is no interference between unspiked plasma or urine with the emission peak of carbon nanodots.

Optical biosensing of sodium stibogluconate in spiked plasma and urine. The concentration of sodium stibogluconate in real plasma or urine was estimated using a calibration curve or the regression equation of spiked plasma or urine. One milliliter aliquot of plasma or urine was added into a series of centrifuge tubes, spiked with known drug concentrations, and treated with 1 mL of 0.01 M HCl and 1 mL of 10% solution tri-nonylamine in n-hexane and treated as in the above control experiment [23]. Calibration curves were constructed, and the corresponding regression equations were derived to determine the nominal concentration.

Optical biosensing of sodium stibogluconate in patient samples. Seven milliliters of 100 mg/mL Pentostam vial was intramuscularly injected to a healthy volunteer (male 30 years old, 70 kg) after 8 h of fasting. A blank sample was collected from the volunteer before the intramuscular administration. Blood samples were aspirated at different time intervals, 0.5, 1.0, 2.0, 4.0, 8.0, 12.0, and 24.0 h, after intramuscular administration. To obtain plasma samples, the blood samples were withdrawn in sodium citrate (anticoagulant) containing test tubes and centrifuged at 4000 rpm for 30 min. The produced supernatant was collected into test tubes. The same procedures of spiked plasma were performed.

Results and discussion. *Characterization of carbon nanodots and factors affecting its fluorescence.* The TGA of carbon nanodots is displayed in Fig. 1a. The weight loss at a temperature between 130 and 200°C (2.5–4%) is related to the adsorbed water molecules and weakly attached species through weak hydrogen bonds [24]. The weight loss at about 500°C (~5.5%) is related to the surface –OH functional groups decomposition. The sharp weight loss (12–91%) in the range 685–805°C can be related to the oxidation of carbon nanodots, indicating the thermal instability of carbon nanodots at higher temperatures [25]. XRD patterns for carbon nanodots are displayed in Fig. 1b. The reflection band at 2θ=21.68° (002) and the broad band at 2θ=43.1° {100/101} are related to the diffraction of graphite crystal planes [26]. The average particle size was determined for the (002) band using the Debye–Scherrer equation:

$$P_s = \frac{\lambda k}{\beta \cos\theta}, \quad (1)$$

where the X-ray wavelength λ = 1.5405 Å, k = 0.9, and β is the full width at half peak height; P_s was calculated to be 7.5 Å. The Bragg equation was used to calculate the interlayer spacing and found to be 4.34 Å.

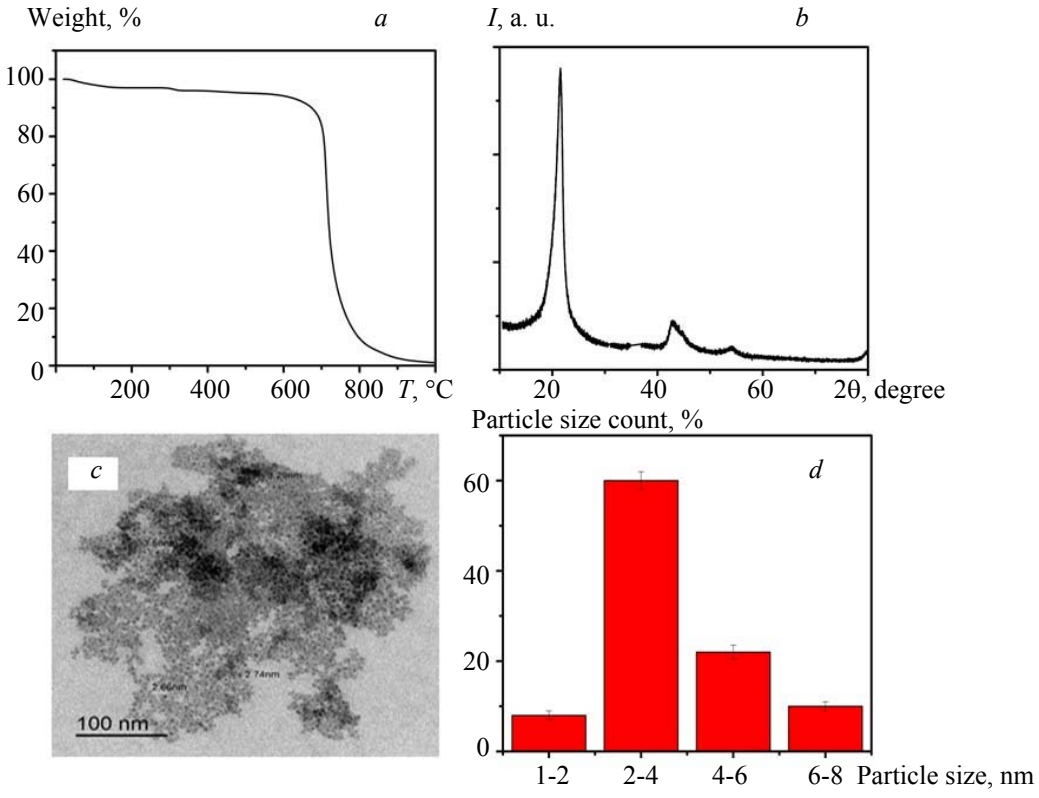

Fig. 1. a) Thermogravimetric analysis curve, b) X-ray diffraction pattern, c) transmission electron microscopy, and d) histogram for the synthetized carbon nanodots.

Figure 1c depicts the TEM image of carbon nanodots, which showed semispherical and smaller nanoparticles with an average diameter of 3.2 nm, as indicated in the histogram (Fig. 1d). Based on the histogram constructed using100 particles in different micrograph regions, we found that about 60% of carbon nanodot particles are located between the 2 and 4 nm particle size; the same result was observed by De and Karak [27]. The selected area electron diffraction (SAED) patterns of the sample (S1a) revealed a diffused ring confirming the amorphous nature of the prepared carbon nanodots [28, 29]. The EDX analysis of carbon nanodots sample (S1b) shows that surface carbon comprises about 95.4%, while oxygen represents about 4.5% of the total surface atoms.

The chemical functional groups characterization was tested by FTIR (Fig. 2a). FTIR spectrum revealed many peaks at around 3442, 2900, 1735, 1645, and 1235 cm^{-1}, which are related to O–H stretching, C–H stretching, C=O vibration, C=C vibration, and alkoxy C–O–C stretching, respectively. The presence of abundance polar C–O functional groups on the surface of the prepared carbon nanodots confirms its hydrophilicity and good water solubility [30].

Different experimental parameters affecting the fluorescence intensity of carbon nanodots were studied, including the concentration of carbon nanodots, the diluting solvent, and the pH of the medium. The experimental parameters were optimized by changing each in turn while keeping the other one constant. The effect of the carbon nanodots concentrations was investigated using different concentrations ranging from 10 to 40 µg/mL. It was found that the concentration of 20 µg/mL gave the highest emission intensity. A further increase in the concentration results in a constant intensity till 30 µg/mL, after which the intensity begins to decrease. The plateau and the decreased portions in intensity may be related to the inner filter effect and the irregular intensity of the excitation light throughout the solution due to the high concentration [31, 32]. The UV-Visible spectrum for the carbon nanodots solution was recorded to prove the inner filter effect (Fig. 2b).

The diluting solvent effect was also studied by trying different solvents such as water, methanol, and acetonitrile. An aliquot of the stock solution of carbon nanodots was diluted with different diluting solvents to obtain a concentration of 20 µg/mL, and the emission intensity was recorded. The highest intensity was obtained using methanol as a diluting solvent. Different mixtures and ratios of solvents were used to investigate their effect on the fluorescence intensity, where methanol/water mixtures gave higher intensities. It was found that 50±0.5% aqueous methanol (methanol:water, 50:50) gave the highest intensity (Fig. 2c). It is believed that the increased fluorescence intensity upon addition of methanol is due to the decreased external conversion compared to that using water or acetonitrile. The lower vibrational energy gap of methanol than that of water decreases the external conversion and hence increases the fluorescence intensity [33].

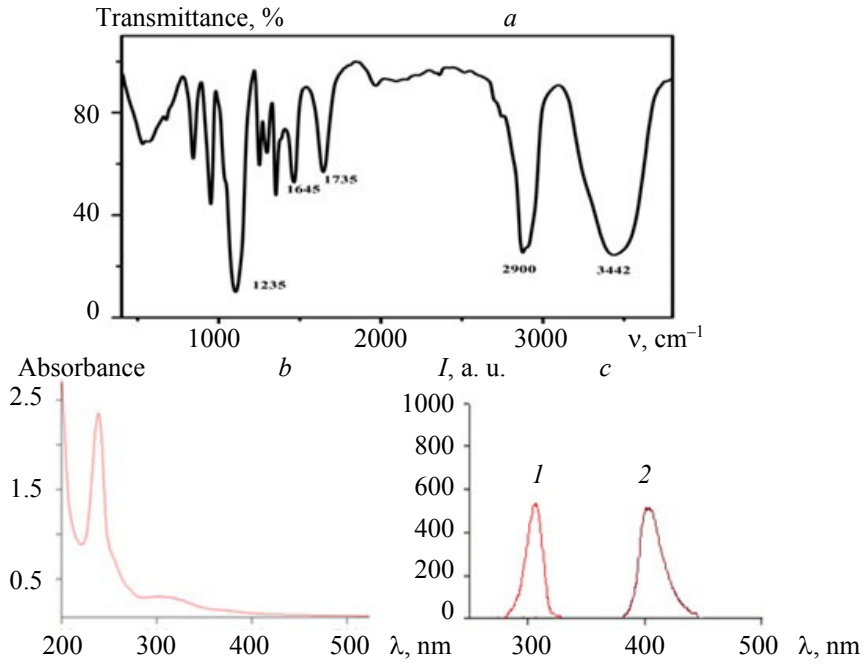

Fig. 2. FTIR spectra: a) UV-Visible and b) and excitation (1) and emission (2) spectra (c) of the prepared carbon nanodots in water: methanol (50:50).

The effect of the pH was also investigated in acidic, neutral, and alkaline media. The fluorescence intensity of carbon nanodots increased in the acidic pH and decreased gradually upon increasing the pH towards the neutral and alkaline regions. The influence of different acidic pH values on the quenching of carbon nanodots fluorescence was studied over the range from 2 to 4.5. The quenching effect increased upon increasing the pH from 2.0 to 2.8, after which the quenching became approximately not affected by a further increase. The optimum pH value was found to be 3.0±0.2, which is related to the degree of ionization of the functional groups on the carbon nanodots surface and the degree of interaction of antimony with the surface functional groups (Fig. 3).

The fluorescent intensity of carbon nanodots was studied in the presence of different cations such as Na^+, K^+, Ca^{2+}, Mg^{2+}, Cu^{2+}, and Fe^{2+}. The monovalent cations Na^+ and K^+ have no effect on the fluorescence intensity. Other heavy metals cations such as Ca^{2+}, Mg^{2+}, Cu^{2+}, and Fe^{2+} display observable interference with antimony on the carbon nanodots at a high concentration. Some of the fluorescence spectra of the carbon nanodots after quenching with 1.0 µg/mL metal cations such as Cu^{2+}, Ca^{2+}, Mg^{2+}, and Fe^{2+} were recorded (S2). It was found that the quenching effect was 84.0, 63.6, 64.1, and 50.0% for Cu^{2+}, Ca^{2+}, Mg^{2+}, and Fe^{2+}, respectively. But these interferences were overcome by the unique selective extraction method of sodium stibogluconate through the ion-pairing with trinonylamine. All organic compounds that may be co-extracted with the drug were digested by refluxing with concentrated sulfuric acid.

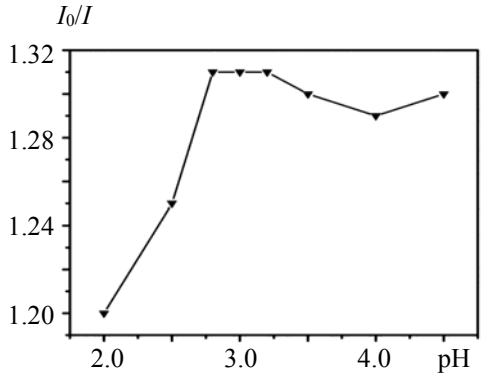

Fig. 3. Effect of the pH on the analysis of sodium stibogluconate by the quenching effect of antimony on the prepared carbon nanodots.

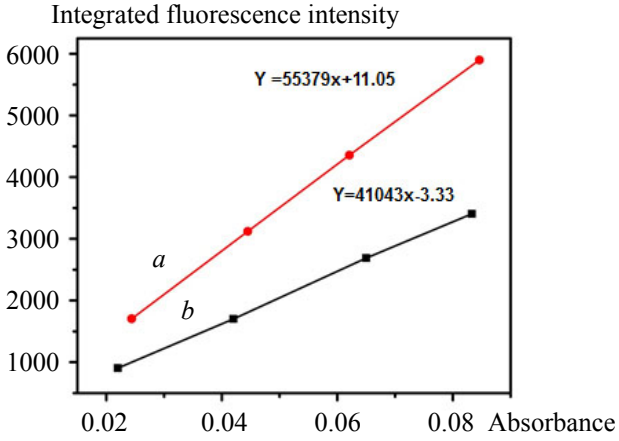

Fig. 4. A plot of the integrated fluorescence intensity *vs* the absorbance of a) 0.1 M quinine sulfate in the sulfuric acid standard solution and b) the prepared carbon nanodots solution.

The quantum yield of the prepared carbon nanodots was calculated utilizing the comparative method using quinine sulfate (0.1 M in sulfuric acid) as a standard solution. Different concentrations of both the standard solution and carbon nanodots were prepared in ultra-pure water, and the absorbance values of these solu-

tions were measured at the excitation wavelength. The fluorescence spectra of the standard and sample solution were recorded, and the integrated fluorescence intensities were calculated. The absorbance was plotted versus the integrated fluorescence intensity, and the gradients of both curves were determined as shown in Fig. 4. The quantum yield was calculated using the following formula:

$$\Phi_x = \Phi_{st}\left(G_x / G_{st}\right)\left(\eta_x^2 / \eta_{st}^2\right), \quad (2)$$

where Φ, G, and η are the fluorescence quantum yield, gradient of the plot of the integrated fluorescence intensity against the absorbance, and the refractive index of the solvent, respectively, while the subscripts x and st refer to the sample and standard, respectively. Application of Eq. (2) revealed that the quantum yield of the prepared carbon nanodots was 40% if the quantum yield of the standard quinine sulfate was 54%. Both quinine sulfate and carbon nanodots were prepared as highly diluted aqueous solutions and so exhibited the same refractive indices values [34]. The Stern–Volmer equation was applied to discuss the kinetics of photophysical intermolecular deactivation:

$$I_0 / I = (\tau_0 / \tau)e^{v[Q]}, \quad (3)$$

where I_0, τ_0, I, and τ are the emission intensity (I_0, I) and the lifetime in an interacting system (τ_0, τ) in the absence and in the presence of the quencher, respectively; v represents the volume per mole of the chromophore and the quencher at the critical interaction distance; [Q] is the concentration of the quencher. The plot (I_0, I) *vs* concentration of stibogluconate (Fig. 5a) was found to be curved upward, which means that the type of quenching is a mixture of static and dynamic quenching. The linearized form of the Stern–Volmer model [35] was applied by plotting log(I_0, I) *vs* concentration of stibogluconate with a correlation coefficient value of 0.9542, as shown in Fig. 5b.

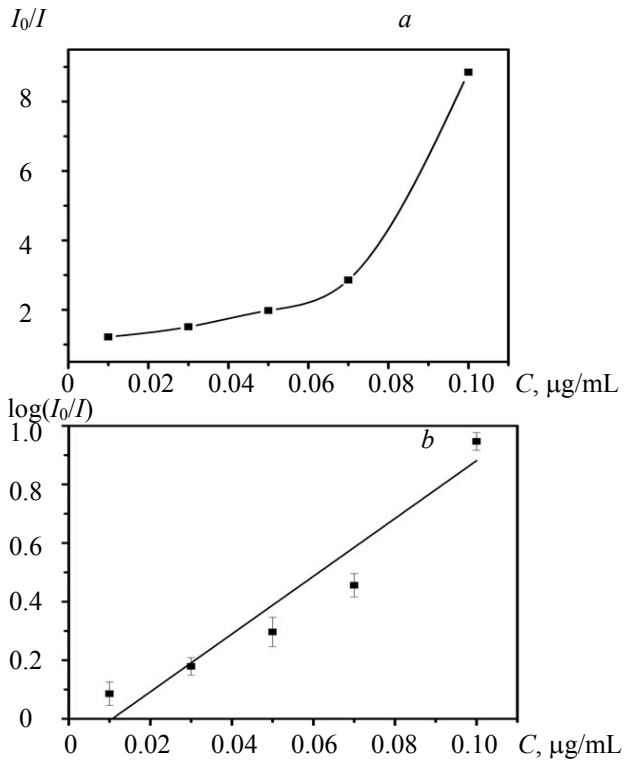

Fig. 5. Stern–Volmer nonlinear (a) and linear (b) plots of carbon nanodots with different concentrations of stibogluconate.

Analytical validation. The method was validated according to the guidelines of ICH [36]. The analytical validation parameters were confirmed with the determination of linearity, range, accuracy, precision, detection quantification limits, and robustness.

Linearity and range of the method. After optimizing the analytical conditions, a calibration curve was constructed by plotting the concentration of sodium stibogluconate against the emission intensity. It was found that the emission intensity was inversely proportional to the concentration of the drug. The calibration curve was linear over the range 0.01–0.10 μg/mL for sodium stibogluconate (Fig. 6), and the regression equation is as follows:

$$I_{Fl} = 573 - 5004\ C, \quad (4)$$

where C is the drug concentration (μg/mL) and $r = 0.9997$ is correlation coefficient.

The obtained regression data such as standard deviations of the slope (S_b), intercept (S_a), and residuals (Sy/x) obtained from the analysis of raw material were statistically analyzed. They were found to be 34.2, 5.0, and 20.30, respectively, and the resulting small values indicate low scattering of the points around the calibration.

Accuracy and precision. The present optical sensor was evaluated by studying the percent relative error (%Er) and percent relative standard deviation precision (%RSD) as indicators for both accuracy and precision [37]. The intraday and interday study results of the sensor are represented in Table 1. Analysis of the data in Table 1 shows (i) the small values of %RSD and %Er were found to have an average value of 0.4 and 0.3, respectively, which indicates good repeatability and high accuracy, and (ii) the obtained values of %RSD and %Er were found to be small with an average value of 0.4 and 0.26, respectively, which indicates good intermediate precision and high accuracy.

The detection (LOD) and quantification (LOQ) limits were calculated from the calibration curve (Fig. 6, Eq. 4) using the equations LOD= $3.3S_a/b$ and LOQ= $10S_a/b$ [37], where S_a and b are the standard deviations of the intercept and slope of the curve. LOD and LOQ were found to be 0.0033 and 0.00999.

The robustness of the present sensor shows that it does not have any observable significant effect on the analysis of performance data with change in the carbon nanodot concentration (20±0.1 μg/mL) and the volume of the diluting solvent aqueous methanol (50±5%) or pH (3±0.2).

The specificity of the present sensing method for antimony was evaluated by examining the interferences of some natural ions such as Na^+, K^+, Ca^{2+}, Mg^{2+}, Cu^{2+}, and Fe^{2+}. The unique extraction procedure through acidification, ion-pairing with trinonylamine, and digestion provides selective extraction of stibogluconate without any other ions or biological compounds.

TABLE 1. Intraday and Interday Precision for the Proposed Method

%Er	%RSD	%Found	Conc. Found, μg/mL	Conc. Added, μg/mL
Intraday				
0.30	0.41	99.50±0.41	0.00995	0.01
0.26	0.38	100.50±0.38	0.05025	0.05
0.32	0.40	100.30±0.40	0.1003	0.10
Interday				
0.25	0.36	99.40±0.36	0.00994	0.01
0.22	0.44	99.80±0.44	0.04990	0.05
0.32	0.41	99.70±0.41	0.09970	0.10

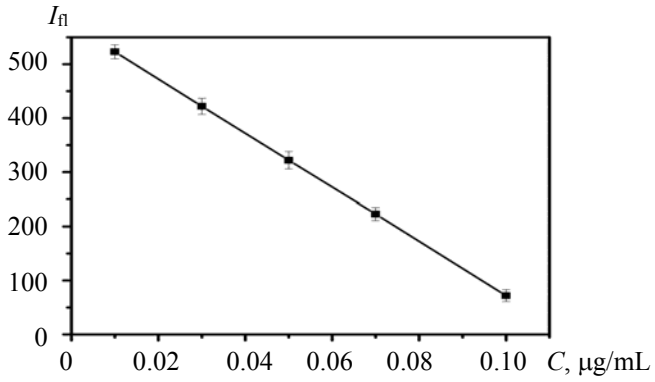

Fig. 6. Calibration curve of the stibogluconate concentration *vs* the fluorescence intensity.

Optical sensing of stibogluconate. Optical sensing of sodium stibogluconate raw material and in Pentostam vial. The sensing of sodium stibogluconate depends on its digestion by concentrated sulfuric acid to release the antimony cation, which acts as a quencher to the carbon nanodot fluorescence. The concentration of the quencher was inversely proportional to the emission intensity of carbon nanodots. The method was applied to the analysis of raw material and Pentostam vial. The results for the sodium stibogluconate determination in both raw material and Pentostam vial are shown in Tables 2 and 3 and exhibit good agreement with the comparison method [14]. The mean percentage of recoveries was 99.99±0.40 and 99.98±0.53 for both raw material and Pentostam vial analyses, respectively. The low working concentration range (0.01–0.10 μg/mL) indicates the high sensitivity of the proposed optical sensor over the reported methods.

TABLE 2. Application of the Proposed and Comparison Methods to the Determination of Stibogluconate Raw Material

Comparison method [13]		Proposed method		Preparation
%Found	Amount taken, μg/mL	%Found*	Amount taken, μg/mL	
100.12	100	99.92	0.01	Stibogluconate
99.50	200	100.59	0.03	
100.33	300	100.32	0.05	
99.70	400	99.64	0.07	
99.60	500	99.52	0.1	
99.85±0.32			99.99±0.40	Mean± SD
		(6.39) *	1.56	*F*-test
		(1.86) *	0.63	*t*-test

*The value of tabulated *t* and *F* (at $p = 0.05$) [37].

TABLE 3. Application of the Proposed and Comparison Methods to the Determination of Stibogluconate in Pentostam Vial

Comparison method [13]		Proposed method		Preparation
% Found	Amount taken, μg/mL	% Found*	Amount taken, μg/mL	
99.81	100	99.72	0.01	Pentostam vial (100 g/mL)
100.6	200	100.52	0.03	
99.5	300	100.71	0.05	
100.41	400	99.42	0.07	
99.44	500	99.55	0.1	
99.95±0.47			99.98±0.53	Mean± SD
		(6.39)*	1.25	*F*-test
		(1.86)*	0.10	*t*-test

*The value of tabulated *t* and *F* (at $p = 0.05$) [37].

Optical biosensing of sodium stibogluconate in spiked biological fluids. Biosensing of sodium stibogluconate represents a challenge due to the difficulty of its extraction from biological fluids. Sodium stibogluconate has very good water solubility but it is insoluble in organic water immiscible solvents, which makes liquid extraction very difficult. This problem was solved by the addition of hydrochloric acid to convert the sodium salt to the parent drug, stibogluconate. The parent drug contains a glucuronic acid moiety, which was ion paired with a long-chain amine trinonylamine. Calibration curves of spiked plasma and urine were constructed to be used for further bioestimation of the drug in real plasma. Table 4 shows the results of the recovery studies from the corresponding calibration curve for spiked plasma and urine. The mean percentage recoveries of the proposed optical biosensor were 99.25±1.86 and 99.60±1.33 for spiked plasma and urine.

TABLE 4. Determination of Stibogluconate in Spiked Biological Fluids by the Proposed Method

Proposed method		Preparation
% Found*	Amount taken, μg/mL	
98.50	0.01	Spiked plasma
101.30	0.03	
101.62	0.05	
97.60	0.07	
97.22	0.1	
	99.25±1.86	Mean± SD
100.50	0.01	Spiked urine
100.32	0.03	
97.80	0.05	
98.30	0.07	
101.20	0.1	
	99.60±1.33	Mean± SD

*Each result is the average of three separation determinations.

Optical biosensing of sodium stibogluconate in patient samples. The high sensitively of the present optical biosensor facilitates the estimation of the studied drug in real human plasma as the working concentration range reaches 0.01 μg/mL. The bioavailability of sodium stibogluconate was determined over different time intervals (0.5, 1.0, 2.0, 4.0, 8.0, 12.0, and 24.0 h) after intramuscular administration of the vial (Fig. 7). The collected plasma samples were analyzed, and the corresponding concentrations were obtained from the regression equation of spiked plasma. The maximum plasma concentration was 9.8 μg/mL after 2 h. Hence, the proposed method is a new validated analytical method for dose monitoring of the studied drug in plasma.

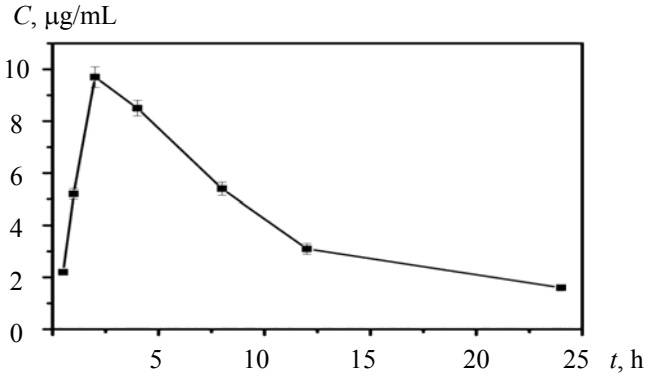

Fig. 7. Plasma concentration of stibogluconate over the period 0.5–24 h.

Conclusions. Carbon nanodots were prepared from garlic peels at 250°C in atmospheric oxygen. The characterization techniques proved that the prepared carbon nanodots with a particle size around of 3.2 nm are amorphous in nature and rich with different C–O functional groups. Carbon nanodots exhibited a good emission fluorescence peak at 420 nm after excitation at 302 nm. The carbon nanodot solution was used in the determination of stibogluconate in plasma and urine. A new method for extraction of stibogluconate from biological fluids was effectively established for the analysis, with a linear range of 0.01–0.10 μg/mL, while 99.89±0.53, 99.25±1.86, and 99.624±1.33 were the percentage recoveries in vials, spiked plasma, and spiked urine, respectively. The analytical parameters, namely accuracy, precision, limit of detection, linear range of detection, and robustness, prove the applicability of carbon nanodots as optical nanobiosensors of stibogluconate in biological fluids. The sensing of stibogluconate was found to be linear over the range 0.01–0.10 μg/mL with percentage recoveries of 99.89±0.53, 99.25±1.86, and 99.624±1.33 in vials, spiked plasma, and spiked urine, respectively.

Disclosure. All authors read and approved the final manuscript. This paper is original and is not under consideration by other publication and has not been published elsewhere. The authors declare that they have no competing interest.

REFERENCES

1. W. Chan, J. Mazwell, X. Gao, E. Baily, M. Han, S. Nie, *Curr. Opinion Biotechnol.*, **13**, No. 1, 40–46 (2002).
2. Y. Lim, W. Shen, Z. Gao, *Chem. Soc. Rev*., **44**, 362–381 (2015).
3. T. T. Dang, V. Mai, Q. Le, N. Duong, Xuan-Dung, *Chem. Phys*., **527**, 110503–110508 (2019).
4. R. Ye, C. Xiang, J. Lin, Z. Peng, K. Huang, Z. Yan, P. Cook, L. G. Samuel, C. Hwang, G. Ruan, G. Ceriotti, O. Raji, A. Marti, M. Tour, *Nature Commun*., **4**, 29–34 (2013).
5. H. Li, X. He, Z. Kang, H. Huang, Y. Liu, J. Liu, S. Lian, C. Tsang, X. Yang, S. Lee, *Angew. Chem. Int. Ed*., **49**, 4430–4434 (2010).
6. Y. Sun, B. Zhou, Y. Lin, W. Wang, K. A. Fernando, P. Pathak, J. Meziani, A. Harruff, X. Wang, H. Wang, G. Luo, H. Yang, E. Kose, B. Chen, L. Veca, S. Xie, *J. Am. Chem. Soc*., **128**, 7756–7757 (2006).
7. Y. Liu, C. Liu, Z. Zhang, *J. Colloid Interface Sci*., **356**, 416–421 (2011).
8. Z. Anwei, Q. Qiang, S. Xiangling, K. Biao, T. Yang, *Angew. Chem. Int. Ed*., **51**, 7185–7191 (2012).
9. C. G. Joaquim, S. Esteves, M. R. Helena, A. Gonc, *Trends Anal. Chem*., **30**, 1327–1336 (2011).
10. H. Li, Y. Zhang, L. Wang, J. Tian, X. Sun, *Chem. Commun*., **47**, 961–963 (2011).
11. A. Cayuela, S. M. Laura, M. Valcarcel, *Anal. Chim. Acta*, **804**, 246–251 (2013).
12. W. Kong, H. Wu, Z. Ye, R. Li, T. Xu, B. Zhang, *J. Lumin*., **148**, 238–242 (2014).
13. https://en.wikipedia.org/wiki/Sodium_stibogluconate#Mechanism_of_action. Accessed on 1st Jan. 2019.
14. British Pharmacopoeia Commission. British Pharmacopoeia 2016, London, TSO (2016).
15. M. S. Bloomfield, A. D. Dow, K. A. Prebble, *J. Pharm. Biomed. Anal.*, **10**, 779–7783 (1992).
16. M. M. S. Junior, L. A. Portugal, A. M. Serra, L. Ferrer, V. Cerdà, S. L. C. Ferreira, *Talanta*, **165**, 502–507(2017).
17. I. López-García, R. E. Rivas, M. Hernández-Córdoba, *Talanta*, **86**, 52–57(2011).
18. L. A. Trivelin, J. J. R. Rohwedder, S. Rath, *Talanta*, **68**, 1536–1543 (2006)
19. Z. Li, Y. Guo, *Talanta*, **65**, 1318–1325 (2005).
20. F. Shakerian, S. Dadfarnia, A. M. H. Shabani, M. N. A. Abadi, *Food Chem.*, **145**, 571–577 (2014).
21. K. Zarei, M. Atabati, M. Karami, *J. Hazard. Mater*., **179**, 840–844 (2010).
22. H. Gaber, B. Rosana, A. Josefa, G. Marta, *Beilstein J. Nanotechnol*., **7**, 758–766 (2016).
23. I. Inci, *Chem. Biochem. Eng. Q*., **16**, No. 4, 81–85 (2002).
24. M. Ashmi, P. Sunil, Th. Mukeshchand, J. Dhanashree, Sh. Madhuri, *J. Mater. Chem. B*, **2**, 698–705 (2014).
25. O. Emil, A. Zhypargul, I. Chihiro, I. Hirotaka, U. Saadat, M. Tsutomu, *J. Nanosci. Nanotechnol*., **15**, 3703–3709 (2015).
26. F. Suárez-García, A. Martínez-Alonso, J. M. Díez Tascón, *J. Anal. Appl. Pyrol.*, **63**, 283–301 (2002).
27. B. De, N. Karak, *RSC Adv*., **3**, 8286 (2013).
28. P. Tathagata, M. Shanid, P. Gopinath, *ACS Omega*, **3**, 831–843 (2018).
29. J. Liang, J. Wanga, K. Yu, K. Song, X. Wang, W. Liu, J. Hou, C. Liang, *Chem. Phys*., **528**, 110538–110544 (2020).
30. L. Mukesh, M. Abou Talib, Kh. Shahnawaz, P. Sunil, W. Hui-Fen, *Microchim. Acta*, **182**, 2173–2181 **(**2015).
31. S. Ashutosh, G. Stephen, *Introduction to Fluorescence Spectroscopy*, Wiley, ISBN 978-0-471-11098-9 (1999).
32. J. R. Lakowicz, *Principles of Fluorescence Spectroscopy*, Kluwer Academic, New York (1999).
33. P. Atkins, J. de Paula, *Atkins' Physical Chemistry*, 9th ed, OUP Oxford (2010).
34. X. Zhai, P. Zhang, C. Liu, T. Bai, W. Li, L. Dai, W. Liu, *Chem. Commun*., **48**, 7955–7957 (2012).
35. G. Gu, C. Chen, Q. Wang, Z. Gao, M. Xu, *J. Appl. Spectrosc*., **86**, No. 4, 618–622 (2019).
36. M. Kazusaki, S. Ueda, N. Takeuchi, Y. Ohgami, *Chromatography*, **33**, No. 2, 65–73 (2012).
37. J. C. Miller, J. N. Miller, *Statistics for Analytical Chemistry*, 4th ed., Ellis-Howood, New York (1993).

SUPPLEMENTARY

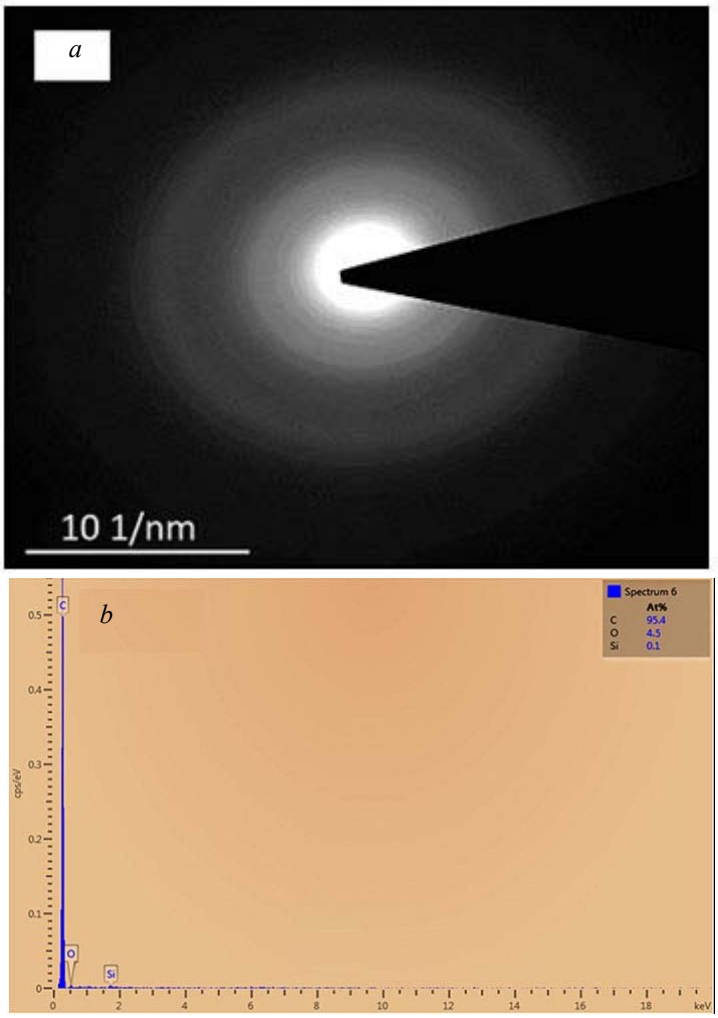

S1: (a) Selected area electron diffraction patterns (SAED), (b) energy dispersive X-ray spectra (EDX) of C-dots.

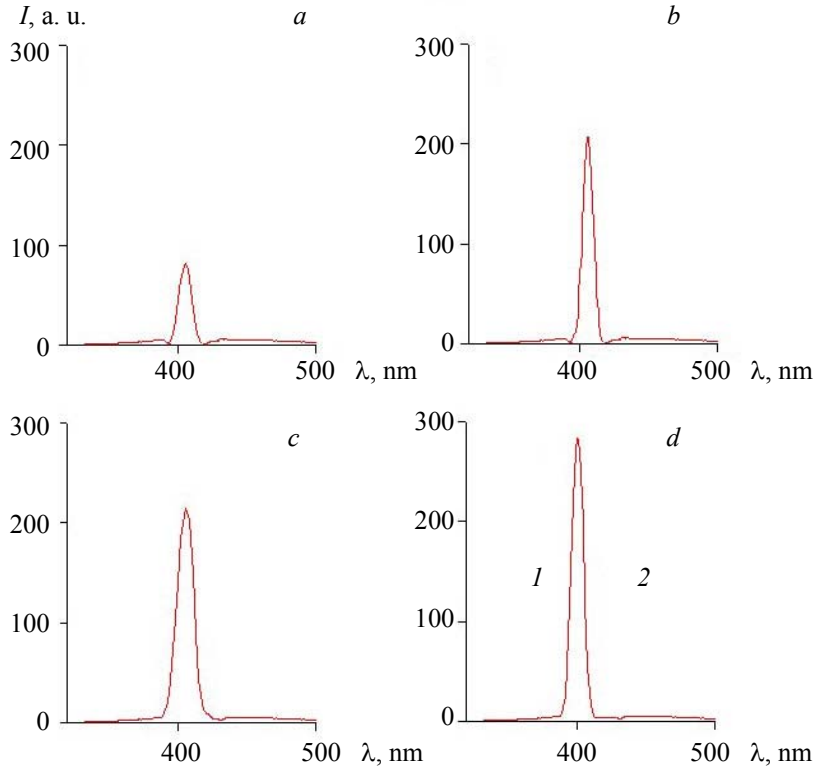

S2: Fluorescence emission spectra of carbon dots after quenching interaction with (a) Cu^{2+}, (b) Ca^{2+}, (c) Mg^{2+}, and (d) Fe^{2+}.